CDF Note 10795

BR($B_s \to J/\psi\phi$) measurement and extraction of the fragmentation fractions

The CDF Collaboration
URL http://www-cdf.fnal.gov
(Dated: April 2, 2012)

A measurement of the ratio of the branching fractions of $B_s \to J/\psi\phi$ to $B^0 \to J/\psi K^*$ based on 9.6 fb^{-1} of data is presented. Samples of reconstructed $B_s \to J/\psi\phi$ and $B^0 \to J/\psi K^*$ collected via the di-muon trigger are utilized. Fitting the B mass distributions with a binned likelihood functions, the yield of 11110 ± 130(stat.) ± 820(sys.) reconstructed $B_s \to J/\psi\phi$ and a yield of 57260 ± 340(stat.) ± 830(sys.) reconstructed $B^0 \to J/\psi K^*$ are measured. These measurements allow a determination of the following quantities:

$$\frac{f_s}{f_d}\frac{Br(B_s \to J/\psi\phi)}{Br(B^0 \to J/\psi K^*)} = 0.239 \pm 0.003(stat.) \pm 0.019(sys.).$$

Using the CDF measurement of f_s/f_d, the ratio of branching fraction to the reference B^0 decay is:

$$\frac{Br(B_s \to J/\psi\phi)}{Br(B^0 \to J/\psi K^*)} = 0.89 \pm 0.01(stat.) \pm 0.07(sys.) \pm 0.11(frag.).$$

Using PDG value for $Br(B^0 \to J/\psi K^*)$ the absolute branching fraction is calculated:

$$Br(B_s \to J/\psi\phi) = (1.18 \pm 0.02(stat.) \pm 0.09(sys.) \pm 0.14(frag.) \pm 0.05(PDG)) \cdot 10^{-3}.$$

We additionally perform the measurement in several ranges of transverse momentum p_T to extract the fragmentation fraction f_s/f_d, where the most recent Belle measurement of $Br(B_s \to J/\psi\phi)$ is used:

$$\frac{f_s}{f_d}\ (all\ p_T\ range) = 0.254 \pm 0.003\ (stat.) \pm 0.020\ (sys.) \pm 0.044\ (BR),$$

$$\frac{f_s}{f_d}\ (6 < p_T < 7.5\ GeV/c^2) = 0.247 \pm 0.010\ (stat.) \pm 0.020\ (sys.) \pm 0.043\ (BR),$$

$$\frac{f_s}{f_d}\ (7.5 < p_T < 9.5\ GeV/c^2) = 0.253 \pm 0.007\ (stat.) \pm 0.023\ (sys.) \pm 0.044\ (BR),$$

$$\frac{f_s}{f_d}\ (9.5 < p_T < 13\ GeV/c^2) = 0.248 \pm 0.006\ (stat.) \pm 0.022\ (sys.) \pm 0.043\ (BR),$$

$$\frac{f_s}{f_d}\ (p_T > 13\ GeV/c^2) = 0.260 \pm 0.006\ (stat.) \pm 0.022\ (sys.) \pm 0.045\ (BR).$$

I. MOTIVATION

The purpose of this analysis is to measure the ratio of branching fractions of $B_s \to J/\psi\phi$ to $B^0 \to J/\psi K^*$ using the relation

$$\frac{Br(B_s \to J/\psi\phi)}{Br(B^0 \to J/\psi K^*)} = A_{rel}\frac{f_d}{f_s}\frac{N(B_s \to J/\psi\phi)}{N(B^0 \to J/\psi K^*)}\frac{Br(K^* \to K\pi)}{Br(\phi \to KK)}.$$

By measuring the ratio of the number of decays, $N(B_s \to J/\psi\phi)/N(B^0 \to J/\psi K^*)$, from data and the relative acceptance, A_{rel}, between the B^0 and B_s from Monte Carlo simulation (MC), the value $Br(B_s \to J/\psi\phi)/Br(B^0 \to J/\psi K^*)$ can be extracted by inputting the ratio of fragmentation fractions f_d/f_s. Moreover, the value of $Br(B_s \to J/\psi\phi)$ can be calculated using the PDG value for $Br(B^0 \to J/\psi K^*)$ [1]. The current PDG value (dominated by the prior CDF measurement) for the Br($B_s \to J/\psi\phi$) is $(1.4\pm0.5)\cdot10^{-3}$ [1, 2]. This measurement will improve significantly upon that result.

In addition of the ratio of branching fraction, the value of f_s/f_d can be measured. The previous equation can be written as follows:

$$\frac{f_s}{f_d}(i) = \frac{Br(B^0 \to J/\psi K^*)}{Br(B_s \to J/\psi\phi)}\frac{Br(K^* \to K\pi)}{Br(\phi \to KK)}\frac{N(B_s \to J/\psi\phi)}{N(B^0 \to J/\psi K^*)}(i)A_{rel}(i),$$

where i means a specific p_T range. Using the PDG value of $Br(B^0 \to J/\psi K^*)$ and the most recent Belle measurement of $Br(B_s \to J/\psi\phi)$ [3], the value of f_s/f_d versus p_T can be extracted. The precision on f_s/f_d will be limited by the large uncertainty on the B_s branching ratio. However, since the branching ratio is a common multiplicative factor across all bins of $p_T(B_s)$ we can still explore the p_T behavior of f_s/f_d with good precision. In other words, this technique won't allow us to extract a precise value of f_s/f_d but it will let us test whether f_s/f_d is flat versus p_T.

II. DATA SAMPLE & MC SAMPLES

The data used in these analyzes are selected from a J/ψ dataset, collected from March 2002 to September 2011 by the CDF Run II detector [4]. It corresponds to an integrated luminosity of 9.6 fb^{-1}. The J/ψ dataset contains events with at least one reconstructed J/ψ selected by dedicated di-muon triggers. The muon identification begins with hits in the muon chambers reconstructed into stubs, and then matched with a reconstructed track in the open-cell wire drift chamber (COT). In addition to the selected J/ψ, two tracks are found to get $B_s \to J/\psi\phi$ and $B^0 \to J/\psi K^*$ candidates. In the $B_s \to J/\psi\phi$ analysis, the two tracks are reconstructed using a kaon mass hypothesis and combined to define a ϕ candidate. The K^* candidate for the $B^0 \to J/\psi K^*$ decay is reconstructed from a pair of tracks using the π and a K mass hypothesis. If two candidates are reconstructed with the same tracks, with the only difference that the kaon and pion hypotheses are swapped, the K^* candidate closest to the PDG value of 896 MeV/c^2 is selected. These preliminary selection criteria for $B_s \to J/\psi\phi$ candidates and $B^0 \to J/\psi K^*$ candidates are listed in Table I. Additional selection criteria optimized for the B_s channel is described in Sec III.

Simulated samples of B^0 and B_s decays are used to optimize event selection, model signal distributions, and assess systematic uncertainties. For our default MC samples, single b hadrons according to momentum and rapidity spectra measured by CDF [4] are generated. For systematic studies, single b hadrons according yo the predicted next-to-leading order QCD calculations [5] is also generated. These hadrons are then decayed using the EVTGEN package [6] and then fed into a GEANT simulation of the CDF detector [7]. The simulated data are then processed and reconstructed in the same manner as the detector data. For both decays is necessary to specify the polarization parameters in the simulation and the 2011 PDG values are used. For systematic acceptance studies additional samples are generated varying the polarization parameters by one standard deviation with respect to their measured values.

III. $B_s \to J/\psi\phi$ ANALYSIS

Optimization of the event selection

The selection criteria is optimized by maximizing $S/\sqrt{S+B}$, where S refers to the number of signal events and B is the number of background events. For the signal sample, a $B_s \to J/\psi\phi$ MC sample is used where the mass candidate falls in the mass range $5.34\,\mathrm{GeV}/c^2 < M_B < 5.4\ \mathrm{GeV}/c^2$. For the background sample, we use $J/\psi\phi$ candidate events from data with the requirement that the reconstructed candidate mass is inside the range $5.45\ \mathrm{GeV}/c^2 < M_B < 5.51\ \mathrm{GeV}/c^2$. This "upper sideband" region contains events kinematically similar to the combinatorial background in the signal region and is not contaminated by residual signal events. We avoid using the sideband below the B_s peak because it could be contaminated with partially reconstructed B decays.
The optimization is done simultaneously over the kaons transverse momenta $p_T(K^-)$ and $p_T(K^+)$, the B_s transverse momentum $p_T(B_s)$, the B_s transverse decay length $L_{xy}(B_s)$, the B_s impact parameter d_0 and the B_s decay kinematic-fit probability. The optimization cuts are $p_T(both(K)) > 0.8\ \mathrm{GeV}/c$, $p_T(B_s) > 6\ \mathrm{GeV}/c$, $L_{xy}(B_s) > 150\ \mu$m, $|d_0|(B_s) < 90\ \mu$m and fit probability greater than 10^{-5}. Figure 1 shows the figure of merits used to chose the selection criteria.

Signal, backgrounds and Fit

For the purpose of extracting the yield of $B_s \to J/\psi\phi$ signal in the invariant mass distributions, an accurate modeling for signal and backgrounds is needed prior to the fit.

The signal contribution is modeled with three Gaussians template obtained from fits to B_s MC. The relative contributions, means and widths from each Gaussian are fixed in the final fit. In general, it is observed that the MC generally underestimates the widths of the mass distribution by approximately 10%. Therefore, the Gaussian widths of the two narrowest Gaussians are multiplied by a scale factor, which is allowed to float in the final fit. The scale factor is not applied to the third Gaussian since it is not expected to be governed by detector resolution effects as the other two. Moreover, a mass shift is added to the means of all Gaussians templates to account for a possible mass mismodeling in the MC.

The $B_s \to J/\psi\phi$ analysis has three primary background contributions: events arising from random associations of charged tracks (combinatoric), $B^0 \to J/\psi K^*$ decays and $B_s \to J/\psi f_0$ decays (physics.) The combinatorial background is resulting from different sources, for example a real J/ψ plus two random tracks, where the J/ψ could be a prompt J/ψ or coming from a B decay. Other sources that could contribute to it are fake J/ψ reconstructed with prompt fake muons or fake muons coming from heavy flavor. The combinatorial background is modeled in the final fit with an exponential function, where the fraction of combinatorial background events and the decay constant are allowed to float.

Since it is possible for $B^0 \to J/\psi K^*$ candidates to pass the $J/\psi\phi$ reconstruction criteria, $B^0 \to J/\psi K^*$ must be considered as a background. A template, consisting in two Gaussians, extracted from simulation is used to model this background. The widths, means and relative contributions from each Gaussian are fixed in the final fit. The constant width of the narrowest Gaussian is multiplied by the same scale factor used in the signals templates. The $B^0 \to J/\psi K^*$ contribution is constrained using data, basically by measuring the $B^0 \to J/\psi K^*$ in the data, and then using simulation to calculate the fraction of those $J/\psi K^*$ events that would show up in the $J/\psi\phi$ signal region.

$B_s \to J/\psi f_0$ events are a not negligible background when $f_0 \to KK$. This contribution is constrained using: the number of $B_s \to J/\psi\phi$ in data; simulation to calculate the fraction of the $J/\psi f_0$ events that would show up in $J/\psi\phi$; the measured value of $(Br(B_s \to J/\psi f_0) \cdot Br(f_0 \to \pi\pi))/(Br(B_s \to J/\psi\phi) \cdot Br(\phi \to KK))$ [8]; and the PDG value of $Br(f_0 \to KK)/Br(f_0 \to \pi\pi)$. Likewise the $B^0 \to J/\psi K^*$ contribution simulation is used to extract the template, consisting in three Gaussians, to model this background.

A binned log likelihood fit is performed to the invariant mass distributions using the templates for signals and the functions described above. The mass distribution in data for $B_s \to J/\psi\phi$, the final fit, and the residuals appear in Fig. 2 and 3. The yield of the $B_s \to J/\psi\phi$ is determined to be 11110 ± 130(stat.).

$N(B_s \to J/\psi\phi)$ systematic uncertainties

Different sources of systematic uncertainties, which can influence the measured of $N(B_s \to J/\psi\phi)$, are discussed below and summarized in Table II.

The modeling of the B_s signal peak can influence the measurement of the yield. To determine the size of the effect that mismodeling has, the fit is repeated with the widths of the three Gaussians floating in the final fit. This results in a shift of 36 in the yield.

The shape of the combinatorial background is another source of systematic uncertainty. In this case, a polynomial is used instead of an exponential. Additional systematic uncertainties of ±35 is included in the final measurement to take into account this effect.

In the likelihood fit, the combinatorial background contribution is allowed to float. A study was done to evaluate how the yield changes if this contribution is fixed in the final fit. The upper sideband in the invariant mass distribution is used to obtain the combinatorial background contribution before the final fit. A systematic uncertainty is included to account for the difference in the yields between this method and the final one. Therefore an additional systematic uncertainty of 101 is included in $N(B_s \to J/\psi\phi)$ value.

In order to study the uncertainties in $B^0 \to J/\psi K^*$ and $B_s \to J/\psi f_0$ contributions, the fraction of candidates that are $B^0 \to J/\psi K^*$ and $B_s \to J/\psi f_0$ are modified $\pm 1\sigma$ from their normal contributions and the fit is performed again. A shift of 41 and 394, respectively, are assigned to cover the size of the uncertainty in these contributions.

At this point, background coming from $B^0 \to J/\psi K\pi$ (s-wave) is not been considered. In order to account for it, the uncertainty on the number of B^0 background is doubled and the difference in the B_s yield, 707 events, is included as a systematic uncertainty.

The different contributions are added in quadrature resulting in a total systematic uncertainty of ± 820 for $N(B_s \to J/\psi\phi)$.

$N(B_s \to J/\psi\phi)$ in p_T ranges

With the purpose of extracting f_s/f_d, the identical measurement is done splitting the sample in different p_T ranges: $6< p_T <7.5$ GeV/c^2, $7.5< p_T <9.5$ GeV/c^2, $9.5< p_T <13$ GeV/c^2 and $p_T >13$ GeV/c^2. The ranges are chosen so that we have approximately equal populated with signal events. Table III summarizes the yields in the complete sample and in the different p_T ranges. Figures 4 and 5 show the invariant mass distributions and fits.

IV. $B^0 \to J/\psi K^*$ ANALYSIS

The procedure to measure the $B^0 \to J/\psi K^*$ yield is very similar to the one used to get the $B_s \to J/\psi\phi$ yield and described in previous section (Sect. III). Any difference is explained below.

Event Selection

The selection criteria used in the $B^0 \to J/\psi K^*$ analysis is the same used for the $B_s \to J/\psi\phi$ analysis with the only different that in this decay we have $K^* \to K\pi$ instead to $\phi \to KK$. The complete list of selection cuts are: $p_T(K)$ and $p_T(\pi) > 0.8$ GeV/c, $p_T(B^0) > 6$ GeV/c, $L_{xy}(B^0) > 150$ μm, $|d_0|(B^0) < 90$ μm and fit probability greater than 10^{-5}.

Signal, backgrounds and Fit

The fitting technique is similar to the $B_s \to J/\psi\phi$ analysis. The yield of $B^0 \to J/\psi K^*$ signal is obtained in a binned likelihood fit to the invariant mass distribution. Again, the $B^0 \to J/\psi K^*$ signal contribution is modeled with three Gaussian templates obtained from fitting $B^0 \to J/\psi\, K^*$ MC. The $B^0 \to J/\psi K^*$ fit contains $B_s \to J/\psi K^*$ signal. For that signal the template used in the final fit is identical to $B^0 \to J/\psi K^*$, except for a shift of 86.8 MeV/c^2

in the mean value of the three Gaussians. This value corresponds to the PDG mass difference between B_s and B^0. The ratio N($B_s \to J/\psi K^*$)/N($B^0 \to J/\psi K^*$) is allow to float in the fit.

The combinatorial background is a common background with the $B_s \to J/\psi\phi$ sample. This background is modeled in the final fit with an exponential function but this time the decay constant is fixed using the upper sideband. This allows a better estimation of another background: the partially reconstruction contribution.

As has been mentioned, another background that emerges is partially reconstructed B-hadrons where a five-body decay occurs where a π, K, or γ is not reconstructed. This background is fitted with an ARGUS function [9]. The ARGUS function cut off parameter is fixed to 5.23 GeV/c^2 and decay constant is fixed to -1.3. These values come from a published CDF result [10].

Likewise the $B_s \to J/\psi\phi$ analysis, $B_s \to J/\psi\phi$ and $B_s \to J/\psi f_0$ events are considered backgrounds in the $B^0 \to J/\psi K^*$ sample. The same methods used to evaluate and model these backgrounds in the $B_s \to J/\psi\phi$ analysis are applied in this analysis.

The invariant mass distribution for $J/\psi K^*$ and the fit result including the different contributions are shown in Fig. 6 and 7. The yield of $B^0 \to J/\psi K^*$ is determined to be 57260 ± 340(stat.).

$N(B^0 \to J/\psi K^*)$ systematic uncertainties

The sources of systematic uncertainty are similar to the other analysis. In this case the uncertainties for the yield are: 427 from the combinatorial background contribution, 392 from the combinatorial background modeling, 579 from the signal modeling, 124 from the $B_s \to J/\psi f_0$ background and 22 from the $B_s \to J/\psi\phi$ contribution. The systematic uncertainties are summarized in Table II. The contributions are added in quadrature resulting in a total systematic uncertainty of ±829. The final value of $N(B_s^0 \to J/\psi\, K^*)$ is 57260 ± 340(stat.) ± 830(sys.).

$N(B^0 \to J/\psi K^*)$ in p_T ranges

Table III summarizes the yields in the complete sample and in the different p_T ranges. Figures 8 and 9 show the invariant mass distributions and fits.

V. ACCEPTANCE CALCULATION

To determine the $Br(B_s \to J/\psi\phi)/Br(B^0 \to J/\psi K^*)$ and the f_s/f_d, the relative acceptances of $B^0 \to J/\psi K^*$ to $B_s \to J/\psi\phi$ need to be determined. MC samples of $B^0 \to J/\psi K^*$ and $B_s \to J/\psi\phi$ are used to extract A_{rel} as follows:

$$A_{rel} = \frac{N(B^0 \to J/\psi K^*\ passed)/N(B^0 \to J/\psi K^*\ generated)}{N(B_s \to J/\psi\phi\ passed)/N(B_s \to J/\psi\phi\ generated)}, \tag{1}$$

where the number of *passed* candidates is simply the number that passed the event selection criteria and the number of *generated* is number of candidates generated by the MC.

The value for A_{rel} are determined to be: A_{rel}(all p_T *range*) = 0.601 ± 0.002 (stat.); A_{rel}(6< p_T <7.5 GeV/c) = 0.520 ± 0.004 (stat.); A_{rel}(7.5< p_T <9.5 GeV/c) = 0.560 ± 0.004 (stat.); A_{rel}(9.5< p_T <13 GeV/c) = 0.596 ± 0.004 (stat.); A_{rel}(p_T >13 GeV/c^2) = 0.672 ± 0.004 (stat.). The statistical uncertainty on the acceptances for B^0 and B_s are determined assuming binomial statistics. These uncertainties are then propagated through using Gaussian uncertainties for A_{rel} and added in as a systematic uncertainty for the branching ratio calculations or the f_s/f_d. Different systematics uncertainties for A_{rel} have being evaluated.

The B_s and B^0 lifetimes play a role in how well A_{rel} is known. In order to evaluate the effect, the default MCs samples are reweighted. The reweighting is performed by normalizing the default lifetime distribution and comparing it to distributions with the lifetimes increased or decreased by 1σ. The maximum deviations of A_{rel} are summarized in Table IV and are taken as systematic uncertainties.

The default B_s and B^0 samples are generated using the p_T spectrum measured in the $B \to J/\psi X$ analysis [11]. Additional samples are produced using the NDE NLO calculation [5]. The change in the p_T spectrum results in small changes in A_{rel} (see Table IV).

To compute a systematic arising from the polarization, different MCs have been generated modifying $\pm 1\sigma$ the parameters Γ_L/Γ and $\Gamma_\perp/\Gamma$. The maximum variations for the B_s and the B^0 are added in quadrature and taken as systematic uncertainties. Table IV includes the systematic uncertainties related to the polarization.

Table IV shows a summary of the systematic uncertainties on A_{rel}. The different contributions are added in quadrature in the total systematic uncertainties.

VI. RESULTS

With the value of A_{rel}, the measurements of the $f_s Br(B_s \to J/\psi\phi)/f_d Br(B^0 \to J/\psi K^*)$ are made to be:

$$\frac{f_s}{f_d}\frac{Br(B_s \to J/\psi\phi)}{Br(B^0 \to J/\psi K^*)} = 0.239 \pm 0.003(stat.) \pm 0.019(sys.).$$

To determine f_s/f_d , the most recent CDF measurement [12] of $f_s/(f_u + f_d) \times Br(D_s \to \phi\pi)$ is combined with the actual PDG value [1] for $Br(D_s \to \phi\pi)$. With the input of $f_s/f_d = 0.269 \pm 0.033$, the ratio of branching fractions to the reference B^0 decays are:

$$\frac{Br(B_s \to J/\psi\phi)}{Br(B^0 \to J/\psi K^*)} = 0.89 \pm 0.01(stat.) \pm 0.07(sys.) \pm 0.11(frag.).$$

The PDG value for $Br(B^0 \to J/\psi K^*)$ is used to calculate the absolute branching fraction:

$$Br(B_s \to J/\psi\phi) = (1.18 \pm 0.02(stat.) \pm 0.09(sys.) \pm 0.14(frag.) \pm 0.05(PDG)) \cdot 10^{-3}.$$

In addition of the ratio of branching fractions the value of f_s/f_d vs p_T can be extracted. The $f_s Br(B_s \to J/\psi\phi)/f_d Br(B^0 \to J/\psi K^*)$ in different p_T ranges are:

$$\frac{f_s}{f_d}\frac{Br(B_s \to J/\psi\phi)}{Br(B^0 \to J/\psi K^*)}\ (6 < p_T < 7.5\ GeV/c^2) \ = \ 0.232 \ \pm \ 0.009\ (stat.) \ \pm \ 0.019\ (sys.),$$

$$\frac{f_s}{f_d}\frac{Br(B_s \to J/\psi\phi)}{Br(B^0 \to J/\psi K^*)}\ (7.5 < p_T < 9.5\ GeV/c^2) \ = \ 0.238 \ \pm \ 0.007\ (stat.) \ \pm \ 0.021\ (sys.),$$

$$\frac{f_s}{f_d}\frac{Br(B_s \to J/\psi\phi)}{Br(B^0 \to J/\psi K^*)}\ (9.5 < p_T < 13\ GeV/c^2) \ = \ 0.233 \ \pm \ 0.005\ (stat.) \ \pm \ 0.020\ (sys.),$$

$$\frac{f_s}{f_d}\frac{Br(B_s \to J/\psi\phi)}{Br(B^0 \to J/\psi K^*)}\ (p_T > 13\ GeV/c^2) \ = \ 0.244 \ \pm \ 0.005\ (stat.) \ \pm \ 0.021\ (sys.).$$

Using the PDG value of Br($B^0 \to J/\psi K^*$) and the most recent Belle measurement of Br($B_s \to J/\psi\phi$) [3], the values of f_s/f_d in different p_T ranges are:

$$\frac{f_s}{f_d}\ (all\ p_T\ range) \ = \ 0.254 \ \pm \ 0.003\ (stat.) \ \pm \ 0.020\ (sys.) \ \pm \ 0.044\ (BR),$$

$$\frac{f_s}{f_d}\ (6 < p_T < 7.5\ GeV/c^2) \ = \ 0.247 \ \pm \ 0.010\ (stat.) \ \pm \ 0.020\ (sys.) \ \pm \ 0.043\ (BR),$$

$$\frac{f_s}{f_d}\ (7.5 < p_T < 9.5\ GeV/c^2)\ =\ 0.253\ \pm\ 0.007\ (stat.)\ \pm\ 0.023\ (sys.)\ \pm\ 0.044\ (BR),$$

$$\frac{f_s}{f_d}\ (9.5 < p_T < 13\ GeV/c^2)\ =\ 0.248\ \pm\ 0.006\ (stat.)\ \pm\ 0.022\ (sys.)\ \pm\ 0.043\ (BR),$$

$$\frac{f_s}{f_d}\ (p_T > 13\ GeV/c^2)\ =\ 0.260\ \pm\ 0.006\ (stat.)\ \pm\ 0.022\ (sys.)\ \pm\ 0.045\ (BR).$$

Figure 10 shows the f_s/f_d result versus $Br(B_s \to J/\psi\phi)$ comparing it with the PDG value of the f_s/f_d and Belle $Br(B_s \to J/\psi\phi)$ result. Figure 11 shows the values of f_s/f_d in the different p_T bins and they are compared to the PDG value 0.269 ± 0.033.

VII. ACKNOWLEDGMENTS

We thank the Fermilab staff and the technical staffs of the participating institutions for their vital contributions. This work was supported by the U.S. Department of Energy and National Science Foundation; the Italian Istituto Nazionale di Fisica Nucleare; the Ministry of Education, Culture, Sports, Science and Technology of Japan; the Natural Sciences and Engineering Research Council of Canada; the National Science Council of the Republic of China; the Swiss National Science Foundation; the A.P. Sloan Foundation; the Bundesministerium für Bildung und Forschung, Germany; the Korean Science and Engineering Foundation and the Korean Research Foundation; the Science and Technology Facilities Council and the Royal Society, UK; the Institut National de Physique Nucleaire et Physique des Particules/CNRS; the Russian Foundation for Basic Research; the Ministerio de Ciencia e Innovación, and Programa Consolider-Ingenio 2010, Spain; the Slovak R&D Agency; and the Academy of Finland.

[1] C. Amsler et. al., *Phys. Lett. B 667, 1*, (2008).
[2] F. Abe et al., *Phys. Rev. D54, 6596-6609* (1996).
[3] Belle result from 2012 LaThuille: http://agenda.infn.it/getFile.py/access?contribId=39&sessionId=7&resId=0&materialId=slides&confId=4116
[4] R. Blair et. al., FERMILAB-PUB-96/390-E, (1996).
[5] P. Nason, S. Dawson and R.K. Ellis, Nucl. Phys. **B 303**, 607, (1988).
[6] D. J. Lange, Nucl. Instrum. Methods A **462**, 152 (2001).
[7] R. Brun *et al.*, CERN Report No. CERN-DD-78-2-REV; R. Brun *et al.*, CERN Programming Library Long Write-up W5013 (1993).
[8] T. Aaltonen et al., *Accepted by Phys. Rev. D*, arXiv:1106.3682v2, (2011).
[9] ARGUS Collaboration, H. Albrecht, *Phys. Lett. B 241, 278*, (1990)
[10] T. Aaltonen et al., *Phys. Rev. D83, 052012*, (2011)
[11] D. Acosta et. al., *Phys. Rev. D71, 032001*, (2005).
[12] T. Aaltonen et. al., *Phys. Rev. D77, 072003*, (2008).

Parameter	$B_s \to J/\psi\phi$ Candidate	$B^0 \to J/\psi K^*$ Candidate
B Mass Range (GeV/c^2)	4.6<Mass<6.2	3<Mass<6.2
B vertex fit χ^2	50	50
B Δz	1.5	1.5
J/ψ Mass (GeV/c^2)	2.8<Mass<3.75	2.8<Mass<3.75
J/ψ vertex fit χ^2	30	30
ϕ Mass (GeV/c^2)	1.0<Mass<1.04	-
K^* Mass (GeV/c^2)	-	0.78<Mass<0.98
ϕ vertex fit χ^2	30	-
K^* vertex fit χ^2	-	20

TABLE I: Preselection cuts for the $B_s \to J/\psi\phi$ Candidates and $B^0 \to J/\psi K^*$ Candidate.

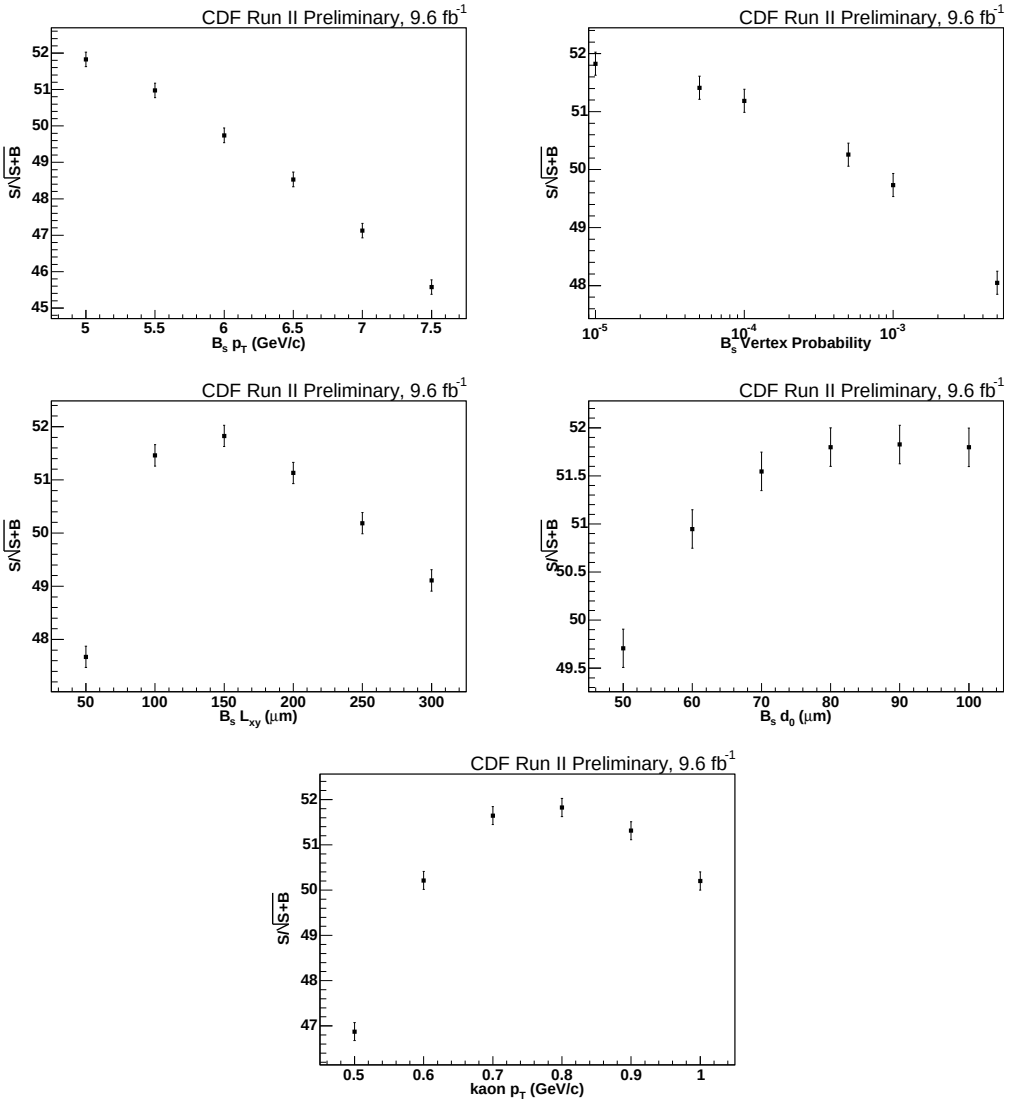

FIG. 1: Figure of merit used in the optimization procedure.

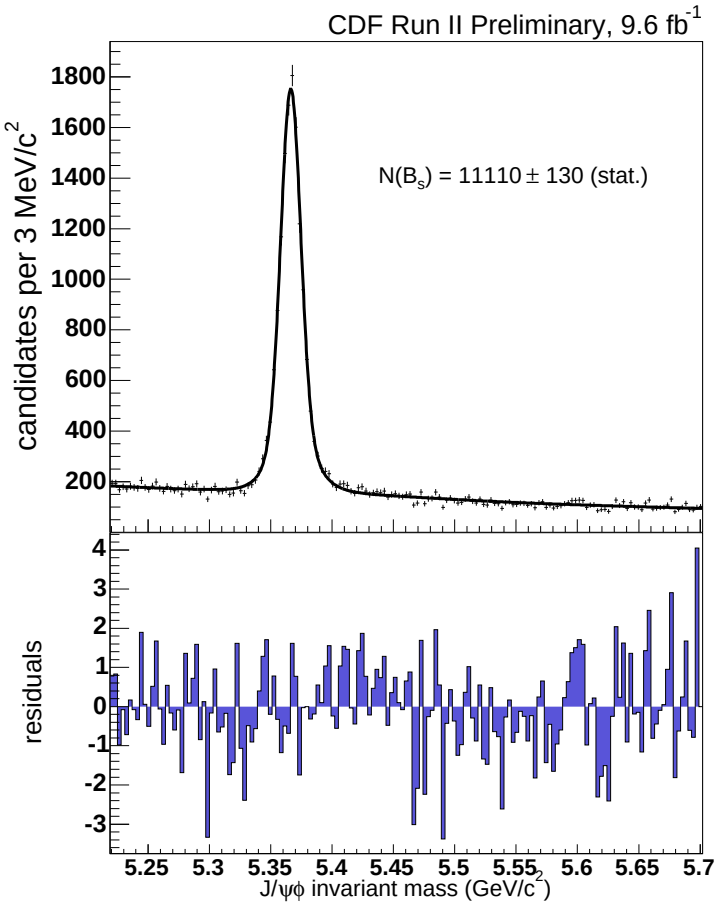

FIG. 2: Invariant mass distribution for $J/\psi\phi$ overlayed with the binned likelihood fit and the residuals.

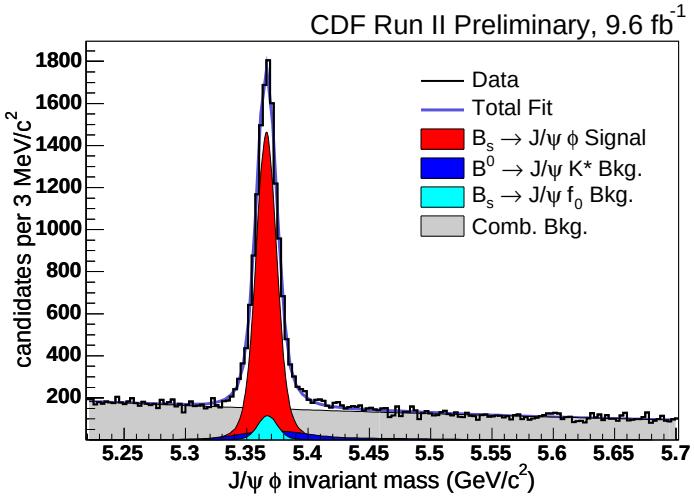

FIG. 3: Invariant mass distribution for $J/\psi\phi$ and fit showing the different contributions.

Source of Systematic Uncertainties	Relative Uncertainty for $N(B_s \to J/\psi\phi)$	Relative Uncertainty for $N(B^0 \to J/\psi K^*)$
Signal Modeling	0.3 %	1.0 %
Combinatorial Background Modeling	0.3 %	0.7 %
Combinatorial Background Contribution	0.9 %	0.7 %
$B^0 \to J/\psi K^*$ Contribution	0.4 %	-
$B_s \to J/\psi\phi$ Contribution	-	0.04 %
$B_s \to J/\psi f_0$ Contribution	3.5 %	0.2 %
$B^0 \to J/\psi K\pi$ Contribution	6 %	-

TABLE II: Systematic uncertainties for the yields.

p_T range (in GeV/c)	$N(B_s \to J/\psi\phi)$	$N(B^0 \to J/\psi K^*)$	N(B_s)/N(B^0)
All p_T range	11110 ± 130 ± 820	57260 ± 340 ± 830	0.194 ± 0.003 ± 0.015
6< p_T <7.5	1600 ± 50 ± 110	7320 ± 150 ± 180	0.218 ± 0.009 ± 0.016
7.5< p_T <9.5	2500 ± 60 ± 190	12000 ± 160 ± 430	0.208 ± 0.006 ± 0.017
9.5< p_T <13	3340 ± 70 ± 280	17460 ± 180 ± 210	0.191 ± 0.004 ± 0.016
p_T >13	3630 ± 70 ± 290	20410 ± 190 ± 420	0.178 ± 0.004 ± 0.015

TABLE III: $N(B_s \to J/\psi\phi)$ yields, $N(B^0 \to J/\psi K^*)$ yields and ratios.

p_T range (GeV/c)	Source B^0 and B_s cτ	Source p_T spectrum	Source Polarization	Total Systematic
All p_T	± 0.012	± 0.006	± 0.011	± 0.017
6< p_T <7.5	± 0.013	± 0.004	± 0.013	± 0.019
7.5< p_T <9.5	± 0.012	± 0.010	± 0.012	± 0.019
9.5< p_T <13	± 0.011	± 0.002	± 0.009	± 0.014
p_T >13	± 0.009	± 0.002	± 0.009	± 0.013

TABLE IV: Relative acceptance systematic uncertainties.

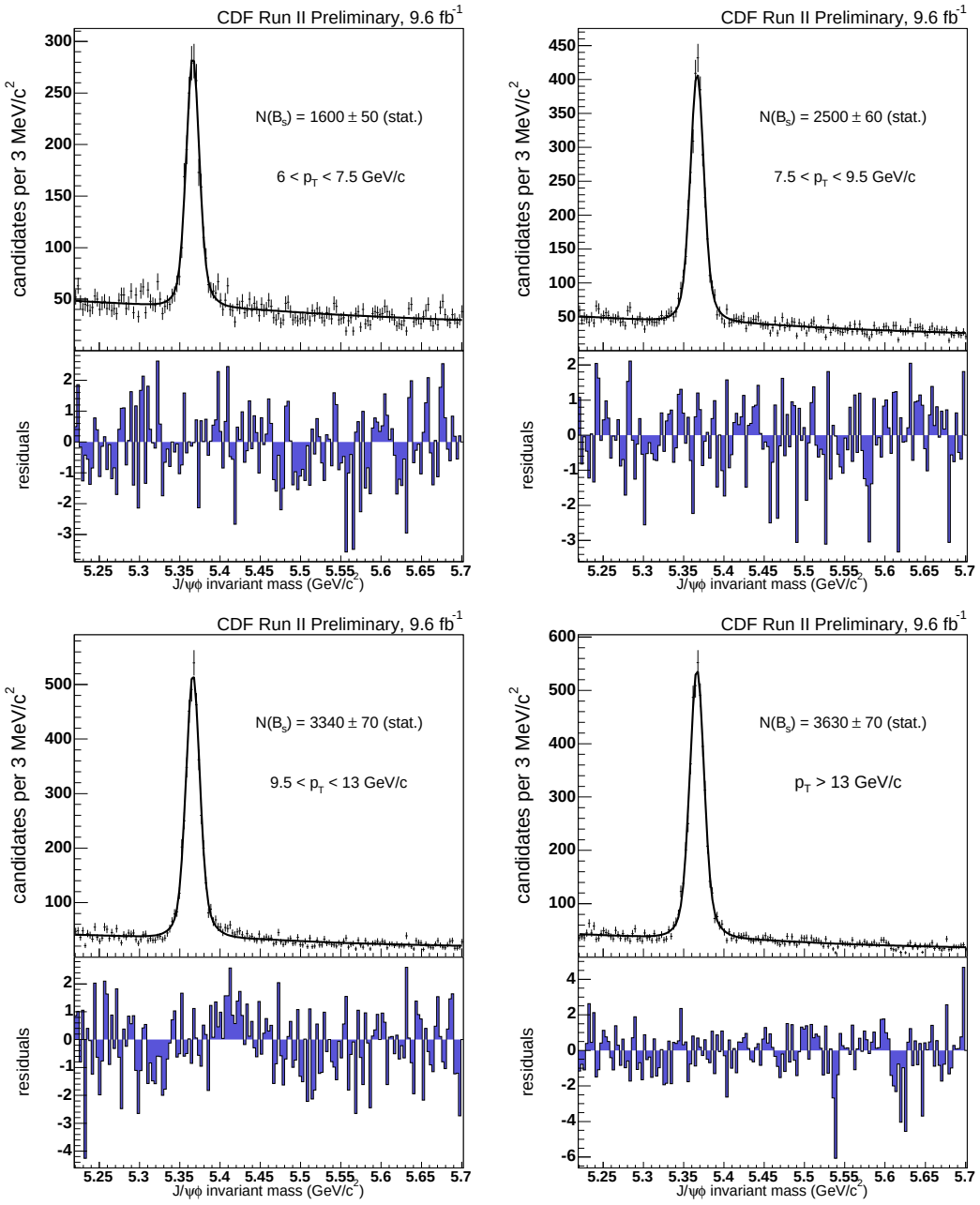

FIG. 4: Mass distributions in different p_T ranges overlayed with the binned likelihood fit and the residuals.

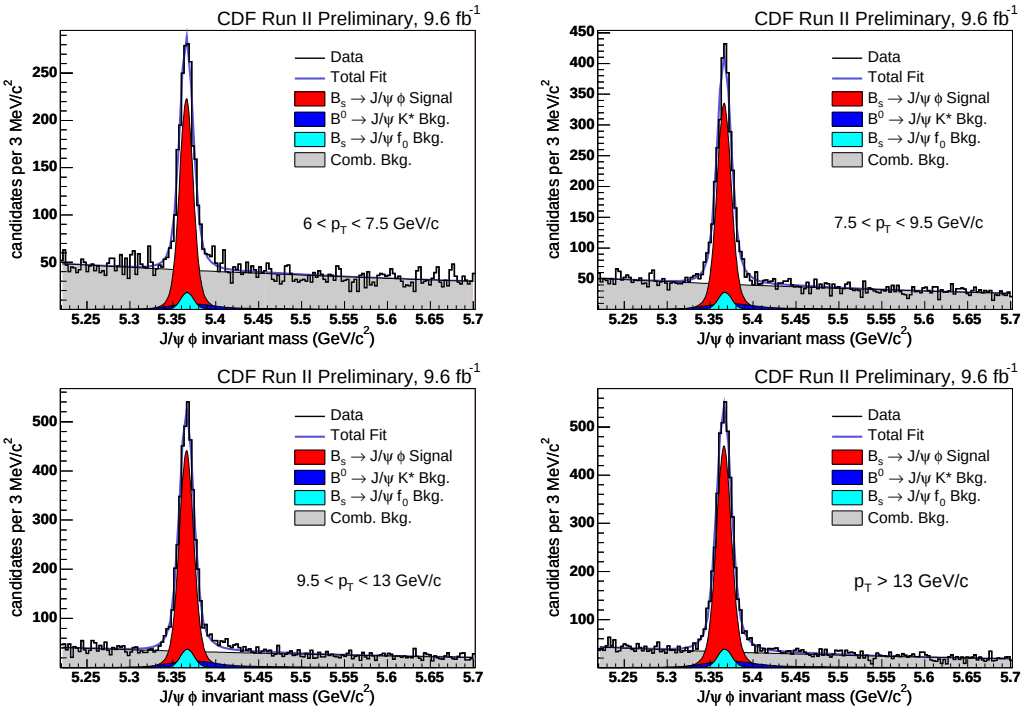

FIG. 5: Mass distribution and fit in different p_T ranges showing the different contributions.

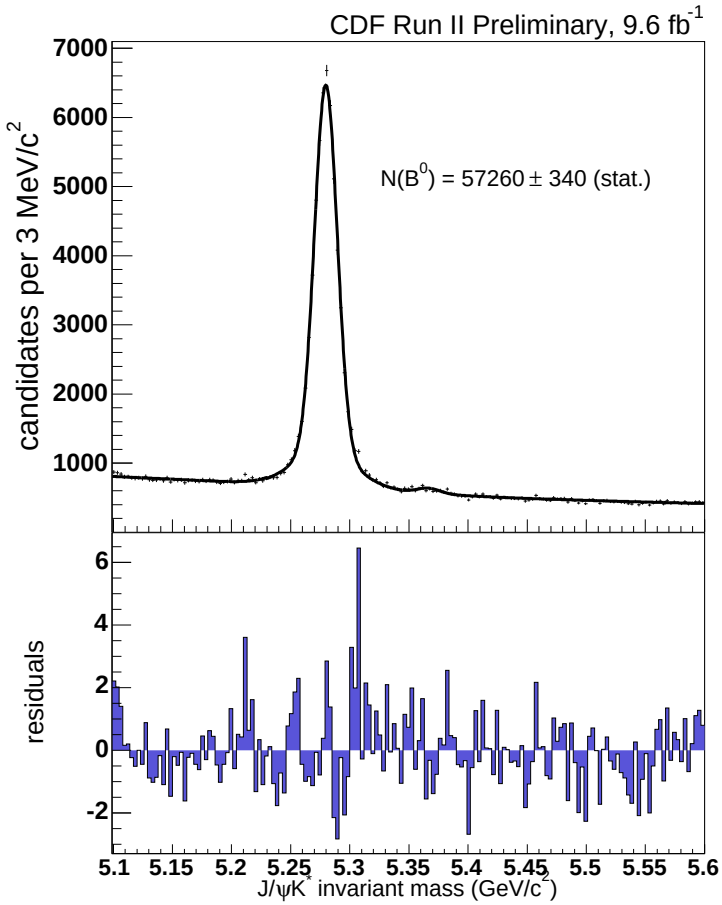

FIG. 6: Mass distribution overlayed with the binned likelihood fit and the residuals.

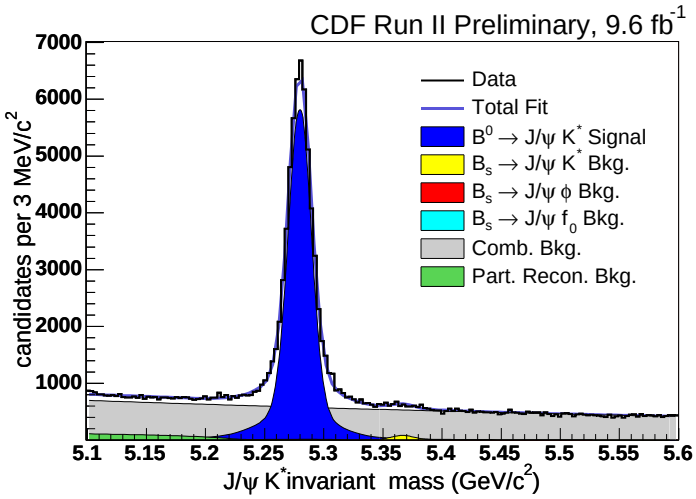

FIG. 7: Mass distribution and fit showing the different contributions.

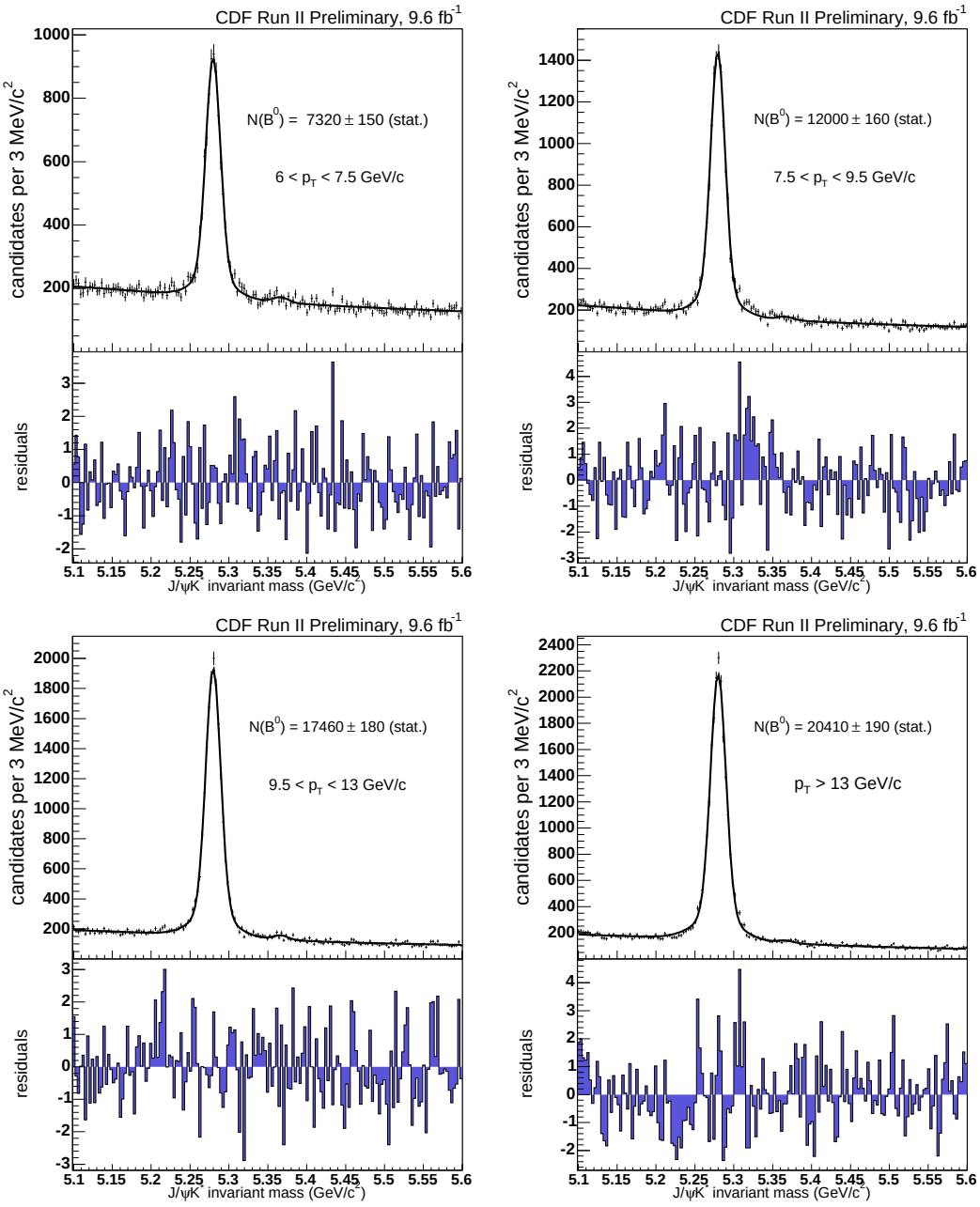

FIG. 8: Mass distributions in different p_T ranges overlayed with the binned likelihood fit and the residuals.

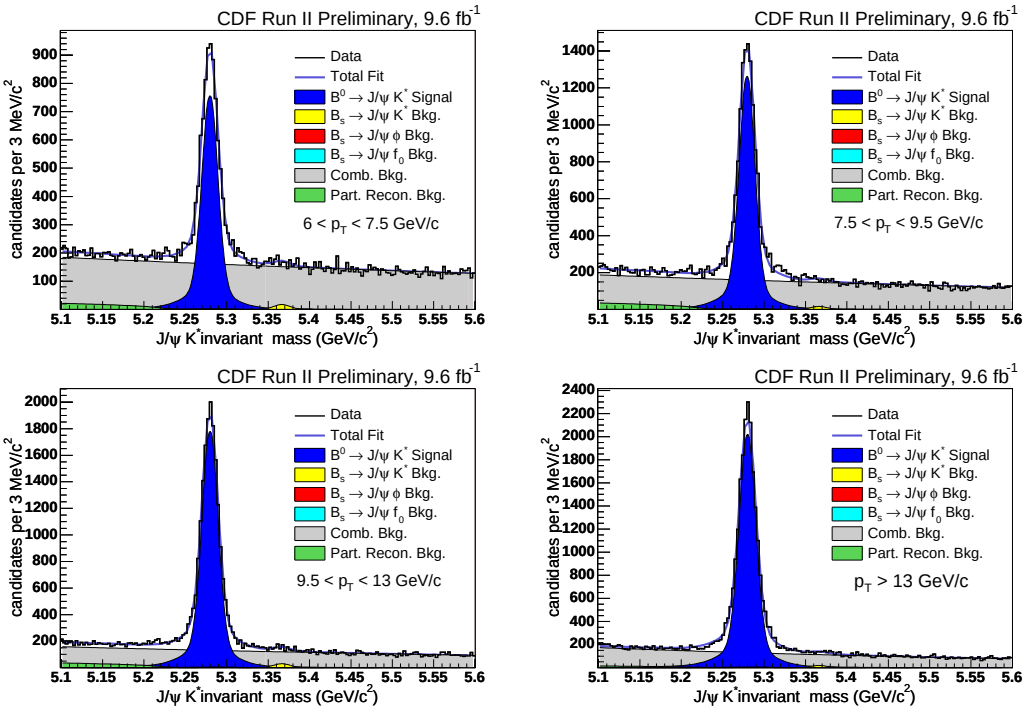

FIG. 9: Mass distribution and fit in different p_T ranges showing the different contributions.

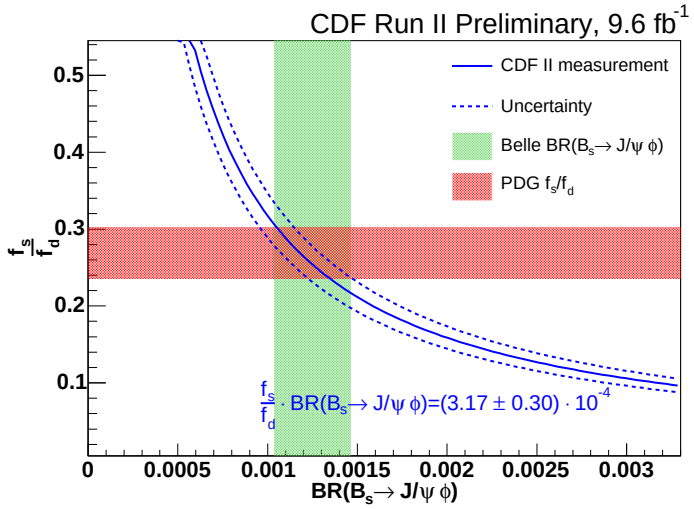

FIG. 10: $f_s/f_d\ Br(B_s \to J/\psi\phi)$ measurement compared to the PDG values.

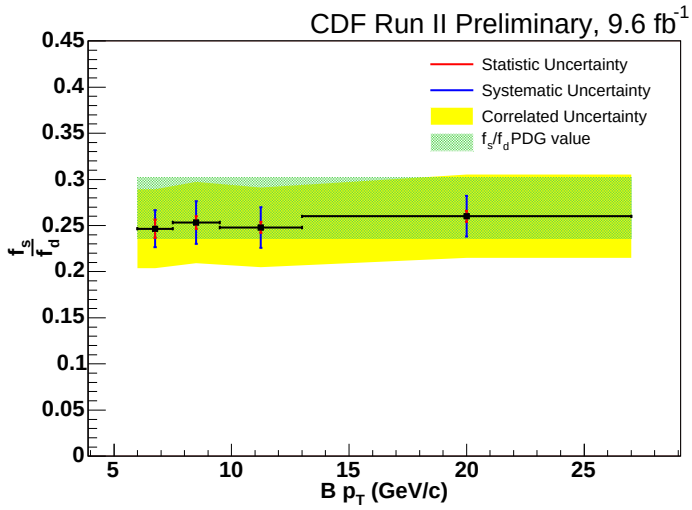

FIG. 11: f_s/f_d in different p_T bins. The measurement is compared to the PDG value.